AERODYNAMIC ANALYSIS OF BUILDINGS USING NUMERICAL TOOLS FROM COMPUTATIONAL WIND ENGINEERING

Alexandre L. Braun[a] and Armando M. Awruch[b]

[a]Graduate Program in Civil Engineering (PPGEC), Federal University of Rio Grande do Sul (UFRGS), Av. Osvaldo Aranha 99, 3° andar, 3492, Porto Alegre-RS, Brasil, allbraun@ig.com.br, http://www.ppgec.ufrgs.br
[a]Graduate Program in Civil Engineering (PPGEC), Federal University of Rio Grande do Sul (UFRGS), Av. Osvaldo Aranha 99, 3° andar, 3492, Porto Alegre-RS, Brasil, awruch@adufrgs.ufrgs.br, http://www.ppgec.ufrgs.br

Keywords: Computational Wind Engineering (CWE), Computational Fluid Dynamics (CFD), Building Aerodynamics, Finite Element Method (FEM), Large Eddy Simulation (LES).

Abstract. This work presents a numerical model based on Computational Wind Engineering (CWE) techniques to simulate the wind action over buildings. CWE deals with application of Computational Fluid Dynamics (CFD) methodologies in classical Wind Engineering problems, which are usually analyzed employing experimental tools in wind tunnels. In Wind Engineering procedures the aerodynamic analysis is performed to investigate effects of the wind action over structures where the structural motion may be neglected. The Navier-Stokes equations for viscous incompressible flows and a continuity equation based on the pseudo-compressibility hypothesis are the governing equations for the fluid analysis. The numerical model to simulate wind flows is obtained applying the explicit two-step Taylor-Galerkin method on the governing equations. Spatial approximations are performed using the Finite Element Method with eight-point hexahedral elements and one-point quadrature, which leads to analytical evaluations of the element matrices. Large Eddy Simulation (LES) is employed to analyze the large scales of turbulent flows and the dynamic model is used for the sub-grid scales modeling. Typical applications on building aerodynamics are simulated in order to demonstrate the accuracy of the present formulation.

1 INTRODUCTION

Computational Wind Engineering (CWE) deals with numerical simulation of classical Wind Engineering problems using numerical algorithms developed by Computational Fluid Dynamics (CFD). Although wind tunnel tests have been traditionally used in the field of Wind Engineering to evaluate the wind action over structures, many investigations are performed now by the computational approach (see Murakami, 1997 and Sthathopoulos, 1997 for detailed information). In this context, applications on building aerodynamics are very useful for validation of CWE codes since highly complicated flow characteristics are usually generated around buildings, such as impingement, separation, reattachment, circulation, vortices, turbulence and 3-D flows.

Building aerodynamics is concerned about the determination of pressure distributions and wind forces acting on building structures. Furthermore, the determination of air flow patterns around buildings or a group of buildings is of great importance for the prediction of wind environmental conditions in urban areas. It is well known that interference effects among adjacent buildings may alter significantly the velocity field in the surroundings of these buildings such that the comfort of pedestrians may be affected. Numerical applications on this subject may be found in Baskaran and Kashef (1996), Sthathopoulos and Baskaran (1996), He and Song (1999) and Tutar and Oguz (2002).

Wind flows are simulated in CWE problems using numerical methods to solve the flow governing equations. Pressure and velocity fields are then created over a spatial domain in which the flow is analyzed. In addition, the dependence of the governing equations on the time domain must be taken into account using some time-marching scheme to solve the transient problem. Numerical models based on the FEM have been developed in the field of CFD over the last forty years and a great success has been reached by these algorithms in many simulations related to engineering applications (see, for instance, Reddy and Gartling, 1994; Gresho and Sany, 1999; Zienckiewicz et al., 2005).

When compared with the sound speed in the air the wind velocity is small for usual CWE applications and therefore, the incompressible flow equations are employed to model these kinds of flows. The mathematical treatment of incompressible flows is subjected to restrictions imposed to the continuity equation by the incompressibility assumption (divergence-free condition on the velocity field). The incompressibility constraint usually leads to implicit treatment of the pressure field, which requires additional storage of computational memory. Moreover, implicit algorithms are not suitable to analyze highly transient problems, as for example, turbulent flows, where the time step is limited by physical reasons. These drawbacks may be circumvented using the pseudo-compressibility hypothesis, introduced by Chorin (1967) to solve incompressible flows by an explicit way. Slight compressibility is justified by natural flows, where the sound is propagated with finite speed, unlike the infinite value predicted by the incompressibility assumption.

Although direct simulation will be an executable task for all Reynolds numbers in a near future, turbulence modeling is still required to represent the effects of small scales over the main flow. Large Eddy Simulation (LES) is recognized as one of the best turbulence models available for CWE applications, since LES can predict the flowfield around a bluff body more accurately than other models do. In the LES formulation, the turbulence's large scales are solved directly and the small scales are reproduced by sub-grid models. In the last decade, computations with the conventional Smagorinsky's sub-grid model (see Smagorinsky, 1963) have been gradually replaced by the dynamic model (see Germano et al. 1991 and Lilly, 1992), which removed some shortcomings of the conventional Smagorinsky's model in the calculation of the eddy viscosity.

In the present paper the flow governing equations are the Navier-Stokes equations and a special form of the mass conservation equation, which is obtained using the pseudo-compressibility hypothesis. Turbulent flows are analyzed using Large Eddy Simulation (LES) with the dynamic model for sub-grid scales. The numerical scheme for the flow analysis is obtained applying the explicit two-step Taylor-Galerkin method (see Kawahara and Hirano, 1983) on the governing equations set. The Finite Element Method is employed for spatial discretizations using the eight-node hexahedrical isoparametric element with one-point quadrature. Typical applications on building aerodynamics are carried out in order to demonstrate the applicability of the present formulation.

2 THE GOVERNING EQUATIONS FOR WIND FLOWS

Wind flows are usually characterized by the following properties:
1) Natural wind streams are considered to be within the incompressible flow range;
2) Wind is always flowing with a constant temperature (isothermal process);
3) Gravity forces are neglected in the fluid equilibrium;
4) Air is considered as a Newtonian fluid.

Considering the properties presented above and in the absence of structural motion (aerodynamic analysis), the flow governing equation are defined in a classical Eulerian kinematical description by the following expressions (see, for instance, Schlichting, 1979):

a) Momentum conserving equations – the Navier-Stokes equations:

$$\frac{\partial v_i}{\partial t} + v_j \frac{\partial v_i}{\partial x_j} = -\frac{1}{\rho}\frac{\partial p}{\partial x_j} + \frac{1}{\rho}\frac{\partial \sigma_{ij}}{\partial x_j} \qquad (i,j=1,2,3) \quad \text{in } \Omega^f \tag{1}$$

b) Mass conserving equation for pseudo-compressible flows (see Braun and Awruch, 2005 for further information) – the continuity equation:

$$\frac{\partial p}{\partial t} + v_j \frac{\partial p}{\partial x_j} + \rho c^2 \frac{\partial v_j}{\partial x_j} = 0 \qquad (j=1,2,3) \quad \text{in } \Omega^f \tag{2}$$

c) Constitutive equation for Newtonian fluids:

$$\sigma_{ij} = -p\delta_{ij} + \tau_{ij} \quad ; \quad \tau_{ij} = \mu\left(\frac{\partial v_i}{\partial x_j} + \frac{\partial v_j}{\partial x_i}\right) + \lambda \frac{\partial v_k}{\partial x_k}\delta_{ij} \qquad (i,j,k=1,2,3) \tag{3}$$

where v_i are components of the velocity vector in the i direction, x_j are components of the cartesian coordinates vector in the j direction, t indicates the time domain, p is the thermodynamic pressure, ρ is the fluid's specific mass, c is the sound speed in the fluid field and Ω^f is the flow's spatial domain, which is bounded by Γ^{Tf}, δ_{ij} are components of the Kroenecker's delta ($\delta_{ij}=1$ for $i=j$; $\delta_{ij}=0$ for $i\neq j$) and μ and λ are the dynamic and volumetric viscosities of the fluid, respectively.

Neumann and Dirichlet boundary conditions must be specified on Γ^{Tf} to solve the flow problem, which are given by the following expressions:

$$v_i = \bar{v}_i \qquad (i=1,2,3) \quad \text{on } \Gamma^v \tag{4}$$

$$p = \bar{p} \qquad \text{on} \quad \Gamma^p \tag{5}$$

$$\left[-\frac{p}{\rho}\delta_{ij} + \frac{\mu}{\rho}\left(\frac{\partial v_i}{\partial x_j} + \frac{\partial v_j}{\partial x_i}\right) + \frac{\lambda}{\rho}\frac{\partial v_k}{\partial x_k}\right]n_j = \frac{\sigma_{ij}n_j}{\rho} = \overline{S}_i \qquad (i,j,k=1,2,3) \quad \text{on } \Gamma^\sigma$$

(6)

where Γ^v (boundary with prescribed values $\overline{v}_i$ for the fluid velocity field), Γ^p (boundary with prescribed values $\overline{p}$ for the pressure field) and Γ^σ (boundary with prescribed values $\overline{S}_i$ for the fluid boundary tractions) are complementary subsets of the boundary Γ^{Tf}, such that $\Gamma^{Tf} = \Gamma^v + \Gamma^p + \Gamma^\sigma$. In Eq. (6) n_j are components of the unit normal vector **n** at the boundary Γ^σ. Initial conditions for the pressure and velocity fields must be also specified at $t = 0$ to start up the flow analysis.

2.1 The turbulence modeling

Although any viscous incompressible flow can be analyzed with the set of governing equations given above, it is observed that only flows with moderate Reynolds numbers can be in fact simulated using direct simulation, considering the computational capacity of the modern computers. Turbulent flows are very restrictive because the smaller turbulence scales, which are associated to the smaller eddies of the flow field, require computational meshes with very fine definition in order to describe the motion of this flow structures correctly. The turbulence problem is usually solved employing modified governing equations that reproduce the turbulence effects over the main flow statistically. These turbulence effects are represented by means of turbulence models. In this work, LES is used in the turbulence modeling.

In the LES formulation the governing equations are submitted to a spatial filtering process where the flow field is decomposed into large and small scales (or large and small eddies). Large eddies are solved directly with the filtered equations, which are described by field variables associated to the large scales, and eddies smaller than the grid resolution are modeled using turbulence closure models, which are employed in order to represent the small scales effects over the large scales.

The governing equations may be written after the filtering process as follows:

$$\frac{\partial \overline{v}_i}{\partial t} + \overline{v}_j\frac{\partial \overline{v}_i}{\partial x_j} = -\frac{1}{\rho}\frac{\partial \overline{p}}{\partial x_i} + \frac{1}{\rho}\left(\frac{\partial \overline{\sigma}_{ij}}{\partial x_j} + \tau_{ij}^{SGS}\right) \qquad (i,j=1,2,3) \quad \text{in } \Omega^f$$

(7)

$$\frac{\partial \overline{p}}{\partial t} + \overline{v}_j\frac{\partial \overline{p}}{\partial x_j} + \rho c^2\frac{\partial \overline{v}_j}{\partial x_j} = 0 \qquad (j=1,2,3) \quad \text{in } \Omega^f$$

(8)

where τ_{ij}^{SGS} are components of the Reynolds sub-grid stress tensor (which is associated to unsolved sub-grid terms that must be modeled) and overbars indicate large scale variables. The Reynolds sub-grid tensor is usually approximated according to the Boussinesq assumption:

$$\tau_{ij}^{SGS} = \rho\left(\overline{v_i'v_j'}\right) = 2\mu_t\overline{S}_{ij}$$

(9)

where commas indicate sub-grid scale variables, μ_t is the eddy viscosity and $\overline{S}_{ij}$ are components of the strain rate tensor, which are expressed in terms of large scale variables as follows:

$$\overline{S}_{ij} = \frac{1}{2}\left(\frac{\partial \overline{v}_i}{\partial x_j} + \frac{\partial \overline{v}_j}{\partial x_i}\right) \tag{10}$$

The eddy viscosity μ_t must be obtained using some sub-grid scale model. In the present work, this is made employing the dynamic sub-grid scale model. The dynamic model was presented first by Germano et al. (1991) and adjusted later by Lilly (1992).

The eddy viscosity μ_t is usually expressed in the dynamic model as shown below:

$$\mu_t = \rho C(\vec{x},t)\overline{\Delta}^2\left|\overline{S}\right| \tag{11}$$

where $C(\vec{x},t)$ is the dynamic coefficient (with $\vec{x}$ and t indicating space and time dependencies), $\left|\overline{S}\right|$ is the filtered strain rate tensor modulus and $\overline{\Delta}$ is the characteristic dimension of the grid filter, which is associated to element volumes in FEM formulations ($\overline{\Delta}^{ele} = \sqrt[3]{vol^{ele}}$). The dynamic coefficient is updated along the time integration process taking into account instantaneous conditions of the flow field. The expression due to Lilly (1992) is employed here as follows:

$$C(\vec{x},t) = -\frac{1}{2}\frac{\mathcal{L}_{ij}\mathcal{M}_{ij}}{\mathcal{M}_{ij}\mathcal{M}_{ij}} \tag{12}$$

where:

$$\mathcal{L}_{ij} = \left\langle \overline{v}_i \overline{v}_j \right\rangle - \left\langle \overline{v}_i \right\rangle \left\langle \overline{v}_j \right\rangle \tag{13}$$

and:

$$\mathcal{M}_{ij} = \left\langle \overline{\Delta}^2 \right\rangle \left|\left\langle \overline{S} \right\rangle\right| \left\langle \overline{S}_{ij} \right\rangle - \left\langle \Delta^2 \left|\overline{S}\right| \overline{S}_{ij} \right\rangle \tag{14}$$

The solution of Eq. (12) demands two filtering processes on the flow governing equations: the first filtering is associated to the use of the LES formulation, which is related to grid filter $\overline{\Delta}$ and large scale variables represented by overbars ($\overline{\bullet}$). The second filtering is referred to a second filter called test filter $\left\langle \overline{\Delta} \right\rangle$, which must be larger than the first filter $\overline{\Delta}$. Second filtering variables are identified by the symbol $\left\langle \bullet \right\rangle$ and they are computed using the expression below:

$$\left\langle \overline{k} \right\rangle^i = \frac{\displaystyle\sum_{j=1}^{n}\left(\frac{\overline{k}^j}{d_i^j}\right)}{\displaystyle\sum_{j=1}^{n}\left(\frac{1}{d_i^j}\right)} \tag{15}$$

where $\left\langle \overline{k} \right\rangle^i$ is the second filtering value at the nodal point i of a generic variable $\overline{k}$, which is associated to large scales of the first filtering, n is the number of nodal points with direct connectivity to the nodal point i, d_i^j is the distance between the nodal points i and j and $\overline{k}^j$ is the first filtering value of a generic variable k computed at the nodal point j. The second filter arrangement is illustrated in Figure 1.

The characteristic dimension of the second filter at a nodal point i is determined by:

$$\left\langle \overline{\Delta} \right\rangle^{\mathrm{i}} = \sqrt[3]{\sum_{\mathrm{p=1}}^{\mathrm{ne}} vol(\mathrm{p})}$$

(16)

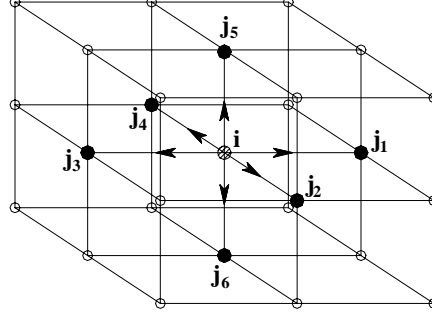where *ne* is the number of elements in the neighborhood of node *i* and *vol*(p) is the volume of the element p.

Figure 1. Second filter arrangement.

The final form of the governing equations with turbulent effects is written as follows:

$$\frac{\partial \overline{v_i}}{\partial t} + \overline{v_j} \frac{\partial \overline{v_i}}{\partial x_j} = -\frac{1}{\rho} \frac{\partial p}{\partial x_j} + \frac{1}{\rho} \frac{\partial}{\partial x_j} \left[(\mu + \mu_t) \left(\frac{\partial \overline{v_i}}{\partial x_j} + \frac{\partial \overline{v_j}}{\partial x_i} \right) + \lambda \frac{\partial \overline{v_k}}{\partial x_k} \delta_{ij} \right] \quad (i,j,k=1,2,3) \quad \text{in } \Omega^{\mathrm{f}}$$

(17)

$$\frac{\partial \overline{p}}{\partial t} + \overline{v_j} \frac{\partial \overline{p}}{\partial x_j} + \rho c^2 \frac{\partial \overline{v_j}}{\partial x_j} = 0 \qquad (j=1,2,3) \quad \text{in } \Omega^{\mathrm{f}}$$

(18)

3   THE NUMERICAL MODEL FOR THE FLOW ANALYSIS

The explicit two-step Taylor-Galerkin scheme is employed in this work for the time discretization of the flow governing equations. Additional information about this numerical model may be found in Kawahara and Hirano (1983) and Braun and Awruch (2003). The algorithm for the flow simulation may be summarized in the following steps:

(1) Calculate $v_i^{n+1/2}$ with:

$$v_i^{n+1/2} = v_i^n +$$

$$\frac{\Delta t}{2} \left\{ -v_j \frac{\partial v_i}{\partial x_j} - \frac{1}{\rho} \frac{\partial p}{\partial x_j} \delta_{ij} + \frac{\partial}{\partial x_j} \left[\frac{\mu + \mu_t}{\rho} \left(\frac{\partial v_i}{\partial x_j} + \frac{\partial v_j}{\partial x_i} \right) + \frac{\lambda}{\rho} \frac{\partial v_k}{\partial x_k} \delta_{ij} \right] + \left(\frac{\Delta t}{4} v_j v_k \right) \frac{\partial^2 v_i}{\partial x_j x_k} \right\}^n$$

(19)

(2) Imposition of the boundary conditions (4) and (6) on $v_i^{n+1/2}$.

(3) Calculate $p^{n+1/2}$ with:

$$p^{n+1/2} = p^n + \frac{\Delta t}{2} \left\{ \left[-v_j \frac{\partial p}{\partial x_j} - \rho c^2 \frac{\partial v_j}{\partial x_j} \right] + \left(\frac{\Delta t}{4} v_i v_j \right) \frac{\partial^2 p}{\partial x_j \partial x_i} \right\}^n$$

(20)

(4) Imposition of the boundary condition (5) on $p^{n+1/2}$.

(5) Calculate the incremental pressure field with $\Delta p^{n+1/2} = p^{n+1/2} - p^n$.

(6) Calculate $v_i^{n+1/2}$ with:

$$v_i^{n+1/2} = v_i^{n+1/2} - \frac{1}{\rho}\frac{\Delta t^2}{8}\frac{\partial \Delta p^{n+1/2}}{\partial x_i} \qquad (21)$$

(7) Imposition of the boundary conditions (4) and (6) on $v_i^{n+1/2}$.

(8) Update the velocity field with $v_i^{n+1} = v_i^n + \Delta v_i^{n+1/2}$, where:

$$\Delta v_i^{n+1/2} = \Delta t\left\{-v_j\frac{\partial v_i}{\partial x_j} - \frac{1}{\rho}\frac{\partial p}{\partial x_j}\delta_{ij} + \frac{\partial}{\partial x_j}\left[\frac{\mu+\mu_t}{\rho}\left(\frac{\partial v_i}{\partial x_j}+\frac{\partial v_j}{\partial x_i}\right)+\frac{\lambda}{\rho}\frac{\partial v_k}{\partial x_k}\delta_{ij}\right]\right\}^{n+1/2} \qquad (22)$$

(9) Imposition of the boundary conditions (4) and (6) on v_i^{n+1}.

(10) Update the pressure field with $p^{n+1} = p^n + \Delta p^{n+1/2}$, where:

$$\Delta p^{n+1/2} = \Delta t\left\{-v_j\frac{\partial p}{\partial x_j} - \rho c^2\left(\frac{\partial v_j}{\partial x_j}\right)\right\}^{n+1/2} \qquad (23)$$

(11) Imposition of the boundary condition (5) on p^{n+1}.

The final form of the numerical model is obtained applying the Bubnov-Galerkin's weighted residual scheme into the FEM context on the discrete forms of the flow governing equations. Eight-node hexahedral elements are used for spatial approximations employing the one-point quadrature technique for the evaluation of element matrices. An efficient method for hourglass control in the fluid mesh is adopted according to the model proposed by Christon (1997).

4   THE NUMERICAL EVALUATION OF AERODYNAMIC COEFFICIENTS

The use of aerodynamic coefficients is very popular in Wind Engineering analyses and many analytical models to describe aerodynamic/aeroelastic phenomena are formulated using this important information. Aerodynamic forces are developed over the body surface of structures immersed in a fluid stream. These forces are usually obtained by the integration of pressures and shear stresses developed on the fluid-structure interface owing to the flow action. The components of the aerodynamic forces in the along-flow and across-flow directions are referred to as drag and lift, respectively.

The aerodynamic coefficients are evaluated in this work using the formulae below:

$$C_{Fx} = \frac{\sum_{i=1}^{NNI}(F_x)^i}{1/2\,\rho V_\infty^2 HW}; \quad C_{Fy} = \frac{\sum_{i=1}^{NNI}(F_y)^i}{1/2\,\rho V_\infty^2 HL}; \quad C_{Fz} = \frac{\sum_{i=1}^{NNI}(F_z)^i}{1/2\,\rho V_\infty^2 WL}$$

$$C_{Mz} = \frac{\sum_{i=1}^{NNI}(F_y\Delta_x - F_x\Delta_y)^i}{1/2\,\rho V_\infty^2 HLW}; \quad C_{Mx} = \frac{\sum_{i=1}^{NNI}(F_z\Delta_y - F_y\Delta_z)^i}{1/2\,\rho V_\infty^2 H^2 L}; \quad C_{My} = \frac{\sum_{i=1}^{NNI}(F_x\Delta_z - F_z\Delta_x)^i}{1/2\,\rho V_\infty^2 H^2 W} \qquad (24)$$

with:

$$\left(\Delta_x\right)^i = X_i - X_g$$

$$\left(\Delta_y\right)^i = Y_i - Y_g \qquad (25)$$

$$\left(\Delta_z\right)^i = Z_i - Z_g$$

where X_i, Y_i and Z_i are Cartesian global coordinates of a nodal point i on the fluid-structure interface, X_g, Y_g and Z_g are Cartesian global coordinates of the body gravity center, V_∞ is the flow reference speed, NNI is the number of fluid nodal points on the body surface and L, W and H are characteristic dimensions related to length, width and height of the immersed body. The aerodynamic forces F_x, F_y and F_z at a nodal point i are obtained by numerical integration of Eq. (6) over the body surface as follows:

$$\left(F_x\right)^i = -\left(t_1\right)^i \left(A_S\right)^i = -\left[\left(\tau_{1j}\right)^i - \left(p\right)^i \delta_{1j}\right]\left(n_j\right)^i \left(A_S\right)^i$$

$$\left(F_y\right)^i = -\left(t_2\right)^i \left(A_S\right)^i = -\left[\left(\tau_{2j}\right)^i - \left(p\right)^i \delta_{2j}\right]\left(n_j\right)^i \left(A_S\right)^i \qquad (26)$$

$$\left(F_z\right)^i = -\left(t_3\right)^i \left(A_S\right)^i = -\left[\left(\tau_{3j}\right)^i - \left(p\right)^i \delta_{3j}\right]\left(n_j\right)^i \left(A_S\right)^i$$

where $\left(A_S\right)^i$ is the influence area of a nodal point i at the fluid-structure interface, which may be obtained by some smoothing procedure taking into account face areas of elements in the neighborhood of the node i, and $\left(n_j\right)^i$ are components of the unit normal vector **n** at the same nodal point i. Although nodal values for the pressure field $\left(p\right)^i$ are obtained by the flow analysis straightforwardly, viscous stresses are variables given at element level in FEM formulations and thus, they must be evaluated at nodal level using smoothing techniques. In this paper the viscous stresses at a nodal point i on the body surface are calculated in the following manner:

$$\tau_{ij}^A = \frac{\sum_{k=1}^{NFC}\left(\tau_{ij}\right)_k \Gamma_k}{\sum_{k=1}^{NFC}\Gamma_k} \qquad (27)$$

where NFC is the number of elements in the neighborhood of a nodal point A at the fluid-structure interface, Γ_k is the face area of the element k and $\left(\tau_{ij}\right)_k$ are shear stress components of the element k, which are evaluated at the finite element center according to the reduced integration technique.

5 NUMERICAL APPLICATIONS

5.1 Wind loads and air flow patterns over a building model

This first numerical application presents the aerodynamic analysis of a building model. The building is submitted to a wind stream with atmospheric boundary layer characteristics in order to obtain circulation patterns of the wind flow around the building and the aerodynamic coefficients. It is important to notice that the present simulation does not consider turbulence

fluctuations in the inflow boundary conditions. Figure 2 shows the referred boundary conditions and the geometrical characteristics of the computational domain, which is constituted by 467840 elements. Physical properties of the wind flow as well as geometrical and numerical constants used in the numerical simulation are presented in Table 1. The present simulation is carried out with a Reynolds number $Re = 9.5 \times 10^4$ ($Re = \rho V_0 D/\mu$).
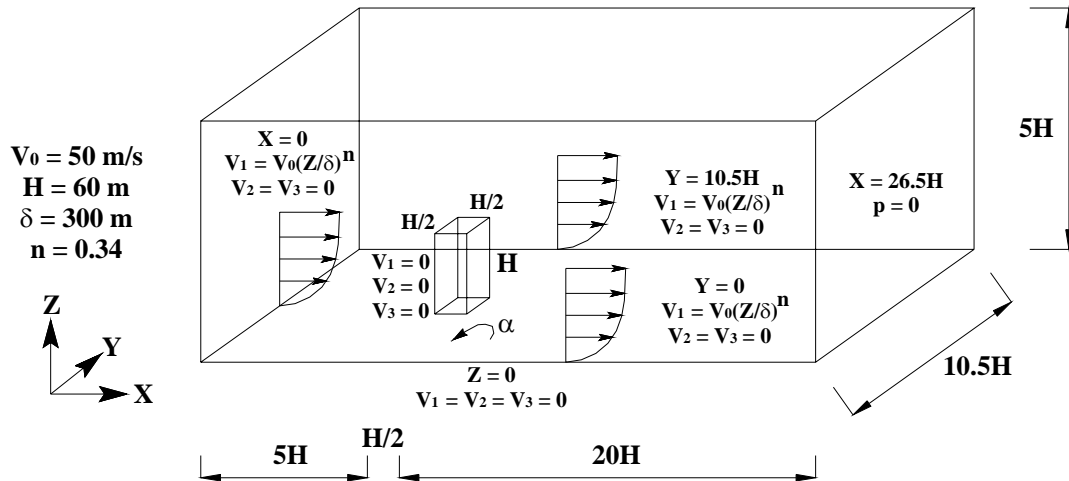

Figure 2. Geometrical characteristics of the computational domain for a building model.

Specific mass (ρ)	1.25 Kg/m^3
Dynamic viscosity (μ)	6.96×10^{-3} Ns/m^2
Volumetric viscosity (λ)	0.0 Ns/m^2
Sound speed (c)	330.0 m/s
Reference velocity – V_0 (avrg. vel. over the bldg. height)	17.6 m/s
Characteristic dimension	30 m
Time step (Δt)	6.5×10^{-4} s

Table 1. Constants employed in the aerodynamic analysis of a building model.

Table 2 presents time-average values of force coefficients obtained by the present work in the aerodynamic analysis of the building model proposed above. These values were calculated from time histories that are referred to drag, lift and moment resultants collected along the numerical simulation. Results referred to the experimental work performed by Akins et al. (1977) in wind tunnel studies are also presented, where a good agreement can be observed between numerical and experimental data.

References	Aerodynamic coefficients					
	C_{Fx}	C_{Fy}	C_{Fz}	C_{Mx}	C_{My}	C_{Mz}
Present work	1.407	0.012	1.340	0.000	0.874	0.024
Akins et al. (1977)	1.457	0.009	1.266	0.000	0.829	0.000

Table 2. Aerodynamic coefficients obtained in the aerodynamic analysis of a building model.

The wind environment conditions around the building model may be evaluated from Figure 3, where instantaneous streamlines obtained by the present simulation are shown. It is observed that the present formulation was able to reproduce most of the circulation patterns

typically developed in the surroundings of high-rise buildings immersed in wind streams with atmospheric boundary layer characteristics. Circulation phenomena such as the development of horseshoe vortices on the floor, recirculation zones behind and in front of the building, conical vortices at the corners of the roof and separation/attachment zones on the lateral/frontal walls were reproduced in accordance with experimental observations (see Peterka et al., 1985 for detailed information about flow circulation around buildings).
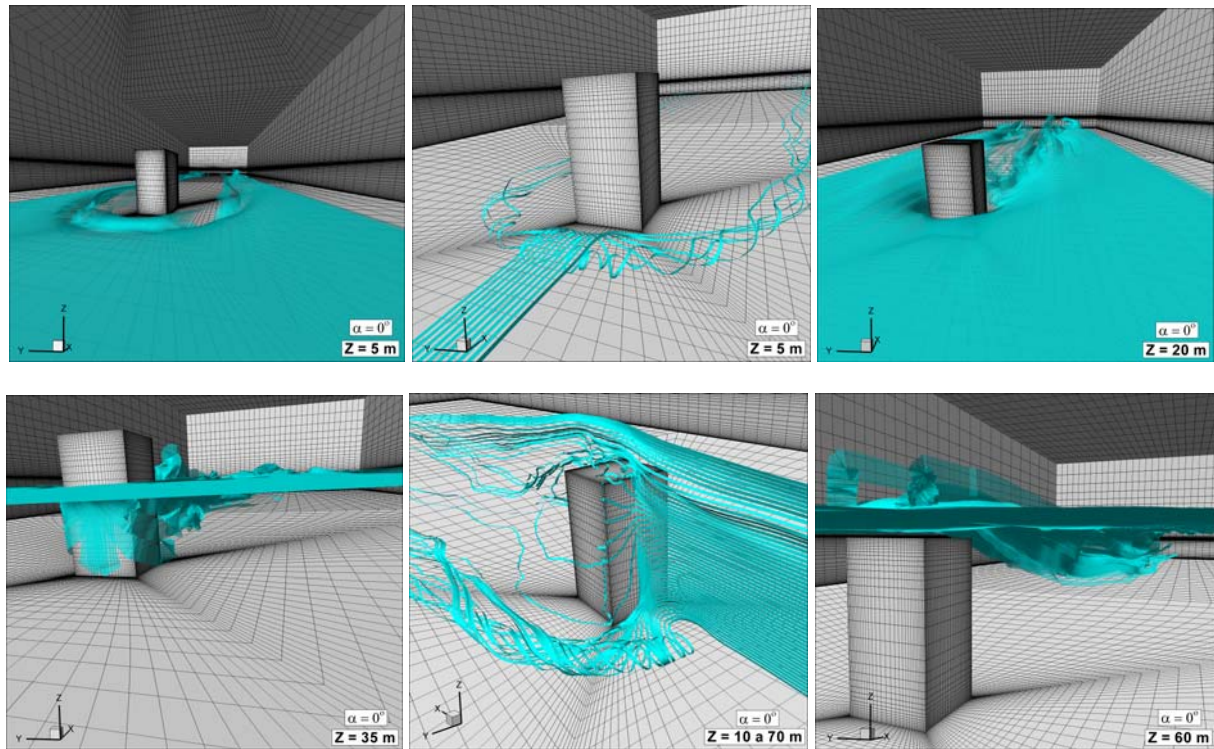

Figure 3. Instantaneous streamlines over the building model.

5.2 Wind loads and air flow patterns over two parallel building models

The present simulation shows the aerodynamic analysis of two parallel buildings with different configurations, which are immersed in a wind flow with atmospheric boundary layer characteristics. Airflow conditions around the buildings as well as aerodynamic forces acting on each building are investigated in this example. A schematic view of the computational domain with the respective boundary conditions may be found in Figure 4. The inflow boundary conditions are represented using a power law mean wind profile without velocity fluctuations. The computational grid is constituted by 752640 elements. Fluid properties are presented in Table 3 with additional constants employed by the numerical algorithm. The numerical analysis is performed with a Reynolds number $Re = 7.9 \times 10^5$.

Table 4 presents time-average values of force coefficients obtained by the present work in the aerodynamic analysis of the parallel buildings proposed above. As in the preceding example, these values were calculated from time histories that are referred to drag, lift and moment resultants collected along the numerical simulation. Unfortunately, experimental results for aerodynamic coefficients are not available in this case.
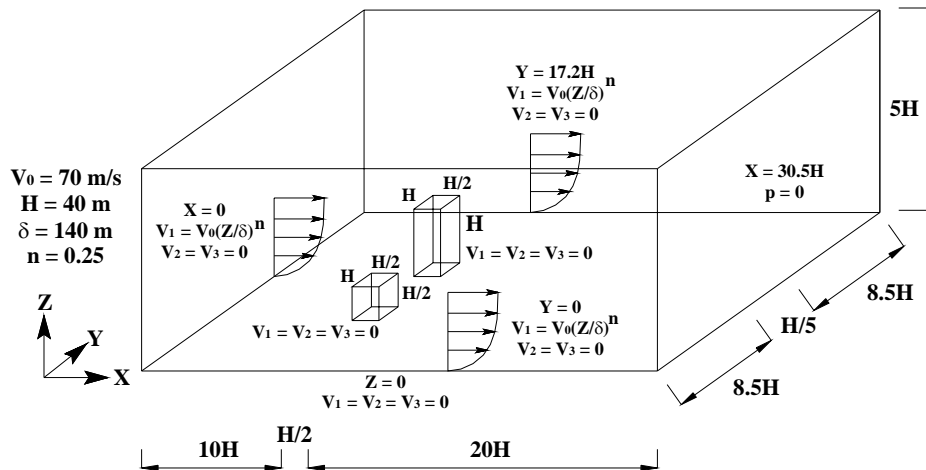
Figure 4. Geometrical characteristics of the computational domain for two parallel building models.

Specific mass (ρ)	1.25 Kg/m^3
Dynamic viscosity (μ)	1.09x10^{-3} Ns/m^2
Volumetric viscosity (λ)	0.0 Ns/m^2
Sound speed (c)	280.0 m/s
Reference velocity – V_0 (avrg. vel. over the bldg. height)	34.7 m/s
Characteristic dimension	20 m
Time step (Δt)	5x10^{-4} s

Table 3. Constants employed in the aerodynamic analysis of two parallel building models.

Buildings	Aerodynamic coefficients					
	CFx	CFy	CFz	CMx	CMy	CMz
Building 1 (H = 40 m)	1.050	-0.045	0.380	0.006	0.055	0.024
Building 2 (H = 20 m)	0.800	-0.400	0.450	-0.019	0.062	-0.048

Table 4. Aerodynamic coefficients obtained in the aerodynamic analysis of two parallel building models.

Figure 5 shows the wind circulation around the building models, which is characterized by the time averaged velocity vector field taken at a height of 2 m above the ground. The velocity field obtained here is compared to the work by Tutar and Oguz (2002), where a reasonable agreement is verified. It is observed that some important characteristics of the flow field were reproduced by the present simulation: (a) development of stagnation zones at the frontal faces of the buildings; (b) development of reverse flow in front of the higher building; (c) flow separation at the frontal corners of both buildings; (d) acceleration of the flow in the passage between the buildings. On the other hand, it is clearly observed that some characteristics were not reproduced adequately. The main difference between numerical and experimental results is found in the frontal region of the parallel buildings, where the area of reverse flow obtained by the present simulation is more pronounced for both buildings. In addition, the flow configuration in the wake of the building models is somewhat different when compared to the reference work. However, these results are justified by the lack of inflow turbulence in the present formulation, which leads to significant modifications in the flow characteristics.
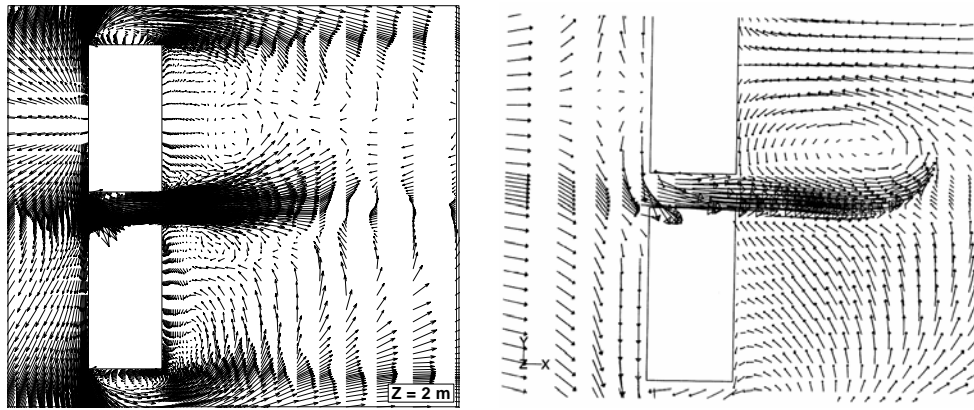
Figure 5. Time averaged velocity vector field around two parallel building models at Z = 2 m.

The wind environment conditions around the parallel buildings are presented in Figure 6, where instantaneous streamlines obtained by the present simulation are shown. The main circulation phenomena of the preceding application can be found in this example. Furthermore, interference effects can be easily observed near the passage between the buildings.
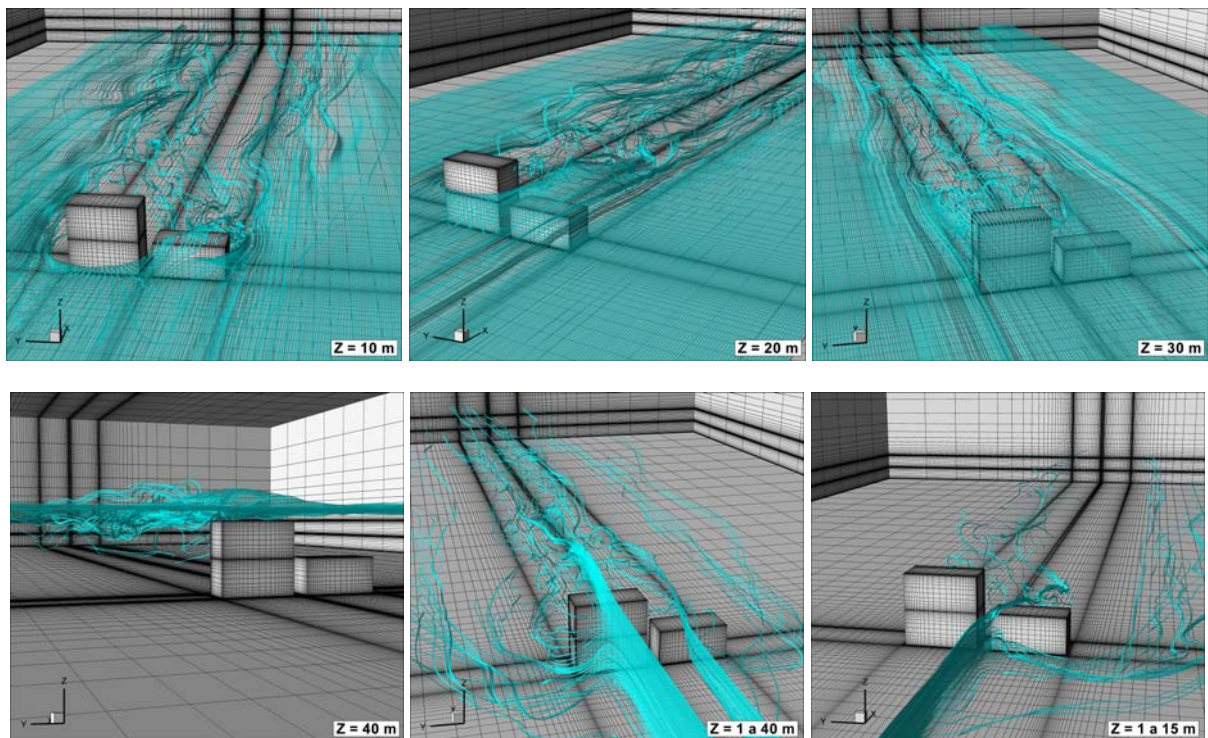

Figure 6. Instantaneous streamlines over two parallel building models.

5.3 Wind environment conditions around a block of buildings

In the present application a typical urban area is selected as a test case for the computation of wind environment conditions around buildings immersed in a flow with atmospheric boundary layer characteristics (except for the turbulence intensity of the incident stream, which is not taken into account by the present formulation). Information about geometrical properties and boundary conditions of the computational domain as well as locations of points

of measurements of wind speeds are presented in detail in Figure 7 with the repective finite element mesh.

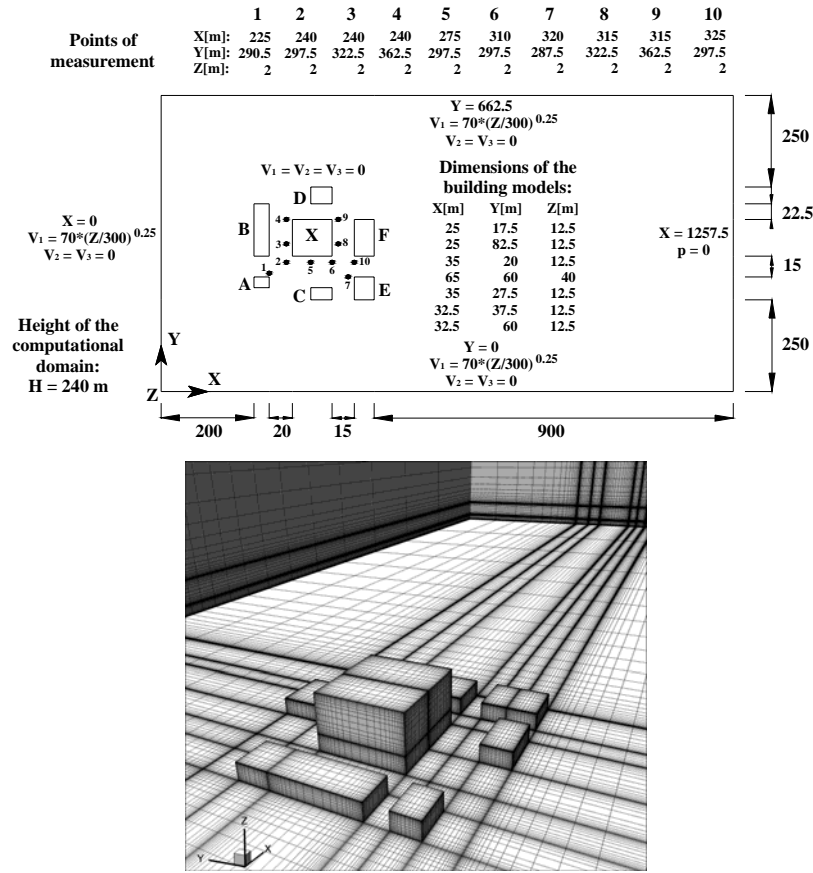| Points of measurement	1	2	3	4	5	6	7	8	9	10
$X[m]$:	225	240	240	240	275	310	320	315	315	325
$Y[m]$:	290.5	297.5	322.5	362.5	297.5	297.5	287.5	322.5	362.5	297.5
$Z[m]$:	2	2	2	2	2	2	2	2	2	2

Figure 7. Geometrical characteristics and finite element mesh of the computational domain for the block of buildings.

The computational grid is constituted by 1268272 elements. Fluid properties are presented in Table 5 with additional constants employed in the numerical analysis. The present simulation is performed with a Reynolds number Re = 10^5 (Re = $\rho V_0 D/\mu$).

Specific mass (ρ)	1.25 Kg/m^3
Dynamic viscosity (μ)	3.17x10^{-2} Ns/m^2
Volumetric viscosity (λ)	0.0 Ns/m^2
Sound speed (c)	230.0 m/s
Reference velocity – V_0 (Z = 40 m)	42.3 m/s
Characteristic dimension – D (= 0.2B)	60 m
Time step (Δt)	6x10^{-4} s

Table 5. Constants employed in the wind environment analysis of a block of buildings.

Time-average pressure fields computed by the present work are shown in Figure 8. It is verified that zones with high pressure are developed in the frontal area of the block of buildings for Z = 5 m and Z = 10 m owing to the action of horseshoe vortices (see Peterka et al., 1985 for further details) near the ground. Zones with complex flow characteristics are also observed between the buildings A and X for Z = 5 m and Z = 10 m, where a recirculating

region with high suction is generated. It is observed that the building X is submitted to larger pressure zones on the frontal surface as well as larger separation areas on the lateral walls due to direct incidence of the wind stream for Z = 25 m and Z = 40 m.
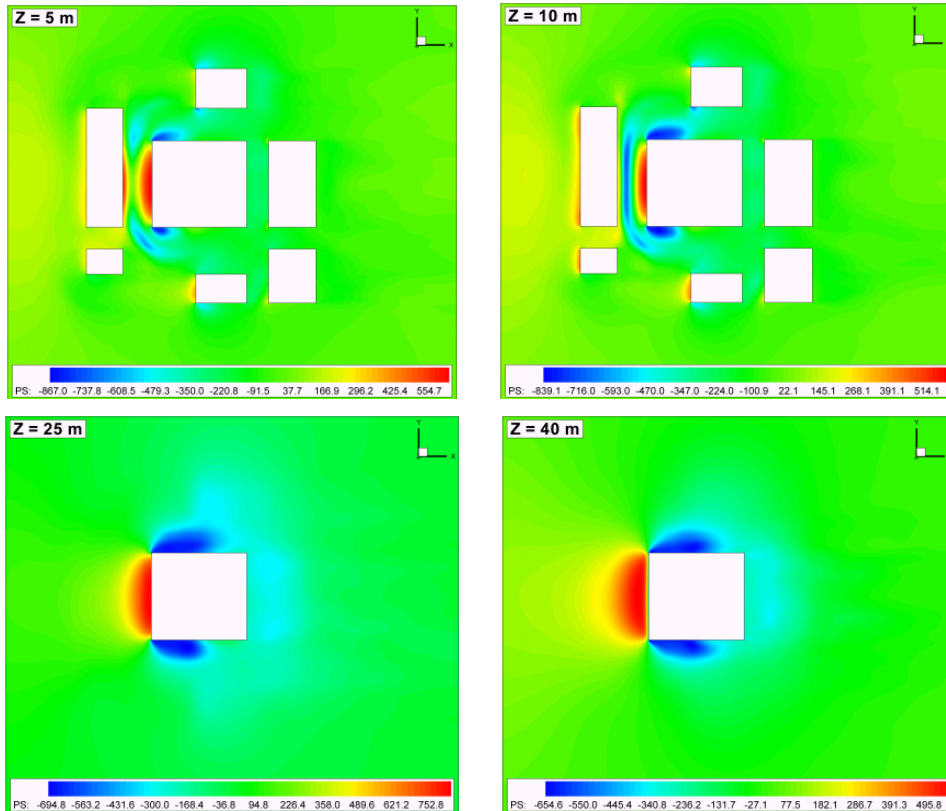

Figure 8. Time-average pressure fields referred to the wind environment analysis of a block of buildings.

The time-average wind speed W ($W = \sqrt{v_1^2 + v_2^2}/V_{in}$; V_{in} = inflow wind speed at Z = 2 m) obtained by the present work at some points of measurement indicated in Figure 7 are shown in Table 6. The present results are compared to experimental and numerical data obtained by Stathopoulos and Baskaran (1996), where a reasonable agreement can be observed.

| Point of measurement | Time-average wind speed W | | |
| | Present work | Stathopoulos and Baskaran (1996) | |
		Numerical	Experimental
1	0.80	0.73	0.98
2	1.49	0.98	1.32
3	0.34	0.57	0.23
4	1.43	1.08	1.28
5	1.26	0.89	1.02
6	1.14	0.81	0.67
7	0.60	0.96	0.76
8	0.27	0.26	0.05
9	0.61	0.58	0.44
10	0.83	0.84	0.64

Table 6. Time-average wind speed W at points of measurements.

6 CONCLUSIONS

A numerical model for building aerodynamics was presented in this work. Some typical applications were analyzed and results obtained by the present algorithm were compared to experimental data from wind tunnel studies. It was verified that the numerical scheme proposed in this paper predicted well most of the physical phenomena referred to the examples simulated here. Insufficient results are related to deficiencies in the boundary layer representation and spatial discretization. Some improvements may be performed in the present formulation in order to obtain a better approach for the physical problem as well as a more efficient code. Suggestions include implementation of a numerical model to consider turbulence fluctuations in the inflow boundary conditions and a numerical algorithm for adaptative meshes.

REFERENCES

Akins, R.E., Peterka, J.A. and Cermak, J.E., Mean force and moment coefficients for buildings in turbulent boundary layers. *Journal of Industrial Aerodynamics*, 2:195-209, 1977.

Baskaran, A., and Kashef, A., Investigation of air flow around buildings using computational fluid dynamics techniques. *Engineering Structures*, 18:861-875, 1996.

Braun, A.L. and Awruch, A.M., Numerical simulation of the wind action on a long-span bridge deck. *Journal of the Brazilian Society of Mechanical Science and Engineering*, 25:352-363, 2003.

Braun, A.L. and Awruch, A.M., Aerodynamic and aeroelastic analysis of bundled cables by numerical simulation. *Journal of Sound and Vibration*, 284:51-73, 2005.

Chorin, A.J., A numerical method for solving incompressible viscous flow problems. *Journal of Computational Physics*, 2:12-26, 1967.

Christon, M.A., A domain-decomposition message-passing approach to transient viscous incompressible flow using explicit time integration. *Computer Methods in Applied Mechanics and Engineering*, 148:329-352, 1997.

Germano, M., Piomelli, U., Moin, P. and Cabot, W.H., A dynamic subgrid-scale eddy viscosity model. *Physics of Fluids*, A3:1760-1765, 1991.

Gresho, P.M. e Sani, R.L., *Incompressible Flow and the Finite Element Method. Advection-Diffusion and Isothermal Laminar Flow*. Sussex, UK: John Wiley & Sons Ltd, 1999.

He, J. and Song, C.C.S., Evaluation of pedestrian winds in urban area by numerical approach. *Journal of Wind Engineering and Industrial Aerodynamics*, 81:295-309, 1999.

Kawahara, M. and Hirano, H., A finite element method for high Reynolds number viscous fluid flow using two step explicit scheme. *International Journal for Numerical Methods in Fluids*, 3:137-163, 1983.

Lilly, D.K., A proposed modification of the Germano subgrid-scale closure method. *Physics of Fluids*, A4: 633-635, 1992.

Murakami, S., Current status and future trends in computational wind engineering. *Journal of Wind Engineering and Industrial Aerodynamics*, 67&68:3-34, 1997.

Peterka, J.A., Meroney, R.N. and Kothari, K.M., Wind flow patterns about buildings. *Journal of Wind Engineering and Industrial Aerodynamics*, 21:21-38, 1985.

Reddy, J.N. and Gartling, D.K., *The Finite Element Method in the Heat Transfer and Fluid Dynamics*. Boca Raton, Florida: CRC Press, 1994.

Schlichting, H., *Boundary-Layer Theory*, 2nd ed., New York: McGraw-Hill Inc., 1979

Smagorinsky, J., General circulation experiments with the primitive equations, I, the basic

experiment. *Monthly Weather Review*, 91:99-135, 1963.

Stathopoulos, T., Computational wind engineering: Past achievements and future challenges. *Journal of Wind Engineering and Industrial Aerodynamics*, 67&68:509-532, 1997.

Stathopoulos, T. and Baskaran, A., Computer simulation of wind environment conditions around buildings. *Engineering Structures*, 18:876-885, 1996.

Tutar, M. e Oguz, G., Large eddy simulation of wind flow around parallel buildings with varying configurations. *Fluid Dynamics Research*, 31:289-315, 2002.

Zienckiewicz, O.C., Taylor, R.L. and Nithiarasu, P., *The Finite Element Method for Fluid Dynamics*, 6th ed. Oxford: Elsevier Butterworth-Heinemann, 2005.